Electromechanical Energy Conversion Systems (EECS),
Niroo Research Institute.
Vol. 1, Issue. 3. Autumn 2019

AN ANALYTICAL PREDICTION FOR MAGNETIC FIELD DISTRIBUTION IN ONE SMPMSM BASED ON SUBDOMAIN MODEL

Seyed Reza Mortezaei[1,2*], Mahmood Hosseini Aliabadi[1,2], Shahram Javadi[1,2]

1- Department of Electrical Engineering, Central Tehran Branch, Islamic Azad University, Tehran, Iran

2- Intelligent Power System and Automation Research Center, Central Tehran Branch, Islamic Azad University, Tehran, Iran

***Corresponding author,** rmortezaeei@gmail.com, mah.hosseini-aliabadi@iauctb.ac.ir*

Abstract

The purpose of this paper is to present an Analytical Predict the Electromagnetic Field Density in surface mounted permanent magnet synchronous motors based on a subdomain field model. In this paper, which is one of a series of four, a 2-d analytical method for predicting field distribution in one SMPMSM is presented. In the presented method, Maxwell's equations have been solved in different regions in pseudo-Cartesian coordinates system taking into account the non-homogeneous boundary conditions. The domain of the magnetic field is divided into four subdomains, viz. magnets, air gap, stator core and outer region. The governing equations and the boundary conditions to the interfaces between these subdomains are formulated in polar coordinate. The analytical prediction is validated by corresponding finite-element method. In future articles, we intend to study the effect of eccentricity on the distribution of magnetic fields in all areas of the motor.

Keywords: Fourier analysis, two-dimensional, subdomain technique, SMPMSM, analytical method

1. INTRODUCTION

With the development of permanent magnet (PM) materials, permanent magnet motors are more and more widely studied and used. these machines Compared with the motors excited by current, offer some advantages such as, low size, high torque densities, high efficiency, high power, and low cost and are increasingly popular in domestic, industrial servos to hybrid electric vehicles, wind power generation and aerospace applications. Accurate analytical computation of the electromagnetic characteristics in the permanent magnet motors is an important tool especially for understanding, design, optimization and maintenance. Over the past decade, there has been dramatic increase in the number of studies which have focused on magnetic field prediction techniques on electrical machines. Among those techniques, subdomain field models have received particular attention. Various categories of magnetic field prediction techniques are Consist of, Lehmann's graphical, Numerical (finite-element, finite-difference, boundary-element, etc.), Equivalent circuit (electrical, thermal, magnetic, etc.) Schwarz–Christoffel mapping (conformal transformation, complex permeance model, etc.), Maxwell–Fourier model (consists of a nonlinear system of N analytical equations solved analytically or numerically). At present, Maxwell–Fourier technique, in comparison with the other techniques, under certain geometrical assumptions, have been found to be useful technique for permit obtaining accurate analytical expressions of the magnetic field and is known as fast for the electromagnetic performance's prediction and is one of the most used analytic approaches with very accurate on the electromagnetic performance's calculation. The Maxwell's equations in Cartesian, cylindrical or spherical coordinates, are solved by using the separation of variables method and the Fourier's series. Various positions have been

advanced in the Maxwell–Fourier analytical models are classified as follows table:

TABLE 7. MAXWELL–FOURIER ANALYTICAL MODELS

Model type	Description
Multi-layer models	Carter's coefficient [1]
	saturation coefficient [2, 3]
	concept wave impedance [4]
	convolution theorem[5]
Eigenvalues model	the method of truncation region Eigen function expansions [6]
	Subdomain technique[1, 2, 7-17]
Hybrid models	the analytical solution combined with numerical methods [18]
	nonlinear magnetic equivalent circuit[19]
tree method	These models are more focused on the global saturation. Some details and (dis)advantages of these techniques can be found in [20].
subdomain technique	

An electrical machine is divided into subdomains and the dominant equation in every subdomain is accurately solved in the method of exact subdomain analysis. The solvable subdomains in this method are consisted of permanent magnets, air gap, and stator core. Exact subdomain analysis method is used for many electrical machines such as brushless PMs and PMSMs. Rahideh and colleagues have proposed a polar axis system for fields analysis of airgap, windings and the distributed magnetic field in a no sloted and brushles motor which operating under an open circuit fault [21]. Koumar and colleagues have suggested an improved analytical method for calculating magnetic field distribution in an BLDC[22]. on the other hand, electrical machines have become more improved in order to identify common faults. So, the technology of identifying electrical machines faults in order to reduce or control mechanical vibrations and to remove extra noise and to enhance equipment in daily lives and industries are considered in this area of study. Therefore, one of the common faults in electrical machines will be mentioned and then, the goal of this research will be noted. Mechanical faults are the types which are caused by flaws in the mechanical parts of electrical motors, such as bearings. The occurrence probability of these faults in electrical motors are between 45 to 55 percent and they are more common than other faults to happen. These faults could be bearing or center escape faults. This type of fault is called eccentricity. In bearing faults, the main cause of machine damage is related to the damage in bearing balls which have different reasons, such as lubricant dirt, too much load and so on. Bearing faults lead to many mechanical effects in machines such as noise increase and vibrations[23, 24]. The rotor and stator eccentricity faults are because of mechanical reasons, their symmetrical centers are displaced. Approximately 80 percent of mechanical faults lead to stator and rotor eccentricity and of course this can happen at the time of rotor production and installation as well[25]. Magnetic tensions cause by electromagnetic and unbalanced magnetic forces and dynamic tensions caused by axis problems and environmental tensions caused by humidity and chemical products and sewer tensions after production and installation and thermal tensions caused by overload and mechanical tensions caused by bearing damages are the main factors of axis problems in permanent magnetic motors. The eccentricity problems are even found in new motors which is called natural and is acceptable up to 10 percent. Therefore, the least rate of this problem is 10 percent. The source of this natural eccentricity problem which is an interesting, sensitive, fate deciding and at the same time, very difficult topic is neglecting when making and installing them[25]. This can be divided into statical and dynamical. In unbalanced statical axis or static eccentricity the rotor rotates around itself which is not compatible with stator geometrical axis. In unbalance dynamic axis or dynamic eccentricity, the rotor is not focused and rotates around stator geometrical axis. In fact there is a third type of unbalanced axis which is a mixture of the previous ones and we witness more of these faults in practice. We call it blended unbalanced axis faults or mixed eccentricity[26]. Vibration analysis, ultrasound analysis, stator frequency or shaft visual analysis can cause the damage in the outer perimeter of the motor. Based on this issue, a lot of comprehensive studies related to these problems could be found[27-38]. Although there have been a lot of valuable research about magnetic factors which are based on some assumptions, it seems that there is no comprehensive analysis in order to identify mechanical and magnetic faults in motors. The purpose of this paper is to present an Analytical Predict the Electromagnetic Field Density in surface mounted permanent magnet synchronous motors (SMPMSM) based on a subdomain field model. In the presented method, Maxwell's equations have been solved in different regions in pseudo-Cartesian coordinates system taking into account the non-homogeneous boundary conditions. The analytical prediction is validated by corresponding finite-element method. In this paper, which is one of a series of four, a 2-d analytical method for predicting field distribution in one SMPMSM is presented. In future articles, we intend to study the effect of eccentricity on the distribution of magnetic fields in all areas of the motor.

2. ANALYTICAL MAGNETIC FIELD MODEL

2.1. Problem Description and Assumptions

Some assumptions are made in this paper, which are usual in many models of the studies as follows:

1) The effect of stator slots and windings are neglected;
2) stator and rotor iron permeability are specified in both analytical and finite element models, and are considered with a linear B-H curve;
3) end effects are neglected;
4) magnets having radially magnetized and a linear second-quadrant demagnetization characteristic;
5) The magnetic field is analyzed in polar coordinates;
6) both the rotor yoke and PM surfaces are perfect cylinders;
7) the axis of the rotor is parallel to the axis of the stator;
8) the permeability of the stator and the rotor back iron is specified.
9) eddy current and saturation effects are neglected

Fig. 1 shows the schematic geometry, subdomains and Symbols of a surface mounted permanent magnet synchronous motors (SMPMSMs) which is used for analysis.

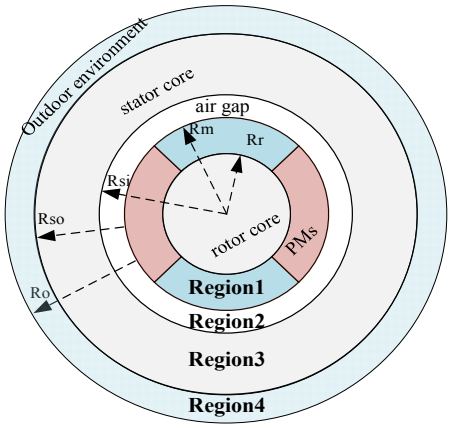

FIG. 1. GEOMETRIC CONFIGURATIONS, FOUR SUBDOMAINS AND SYMBOLS

The magnetic field is produced by an internal rotor which rotates about the axis O_r with the angular velocity of ω.

The axis O_r whirls around the axis O_s with the angular velocity of Ω .

The r-θ coordinate system is fixed to the stator center O_s, while the ρ-ψ coordinate system is attached to the rotor center O_r and rotates about the axis O_r with the angular velocity of ω (**FIG. 2**).

Other main parameters of the geometry are:R_r , the radius of the rotor yoke surface; R_m, the radius of the PM surface; R_{si}, the radius of the stator inner surface; R_{so}, the radius of the stator yoke surface.

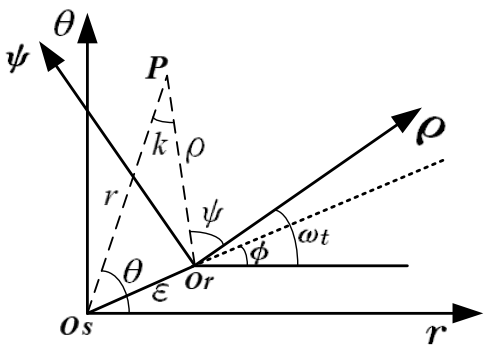

FIG. 2. CORRELATION OF COORDINATES ATTACHED TO THE STATOR AND ROTOR

The field vectors $\vec{B}$ and $\vec{H}$ are coupled by relations as shown in TABLE 8

TABLE 8. RELATIONS BETWEEN OF $\vec{B}$ AND $\vec{H}$ IN DIFFERENT REGIONS

Regions	description	Constructive relationship
Region1	Permanent magnets	$\vec{B}_1 = \mu_0\mu_{rm}\vec{H}_1 + \mu_0\vec{M}$
Region2	Air gap	$\vec{B}_2 = \mu_0\vec{H}_2$
Region3	Stator core	$\vec{B}_3 = \mu_0\mu_{rc}\vec{H}_3$
Region4	Outer region	$\vec{B}_4 = \mu_0\vec{H}_4$

Where, μ_0 is the air permeability, μ_{rc} is the iron relative recoil permeability, μ_{rm} is the PM relative recoil permeability and $\vec{M}$ is the PM magnetization vector, such that its direction dependent on the imparted orientation and magnetization of the magnets.

the amplitude of the magnetization vector is B_r/μ_0. B_r, is the residual flux density of magnets, and the magnetization distribution is shown in **FIG. 3**.

Whereτ_m is the magnet pole-arc, τ_p is the pole-pitch and θ is the angular position with reference to the center of a magnet pole.

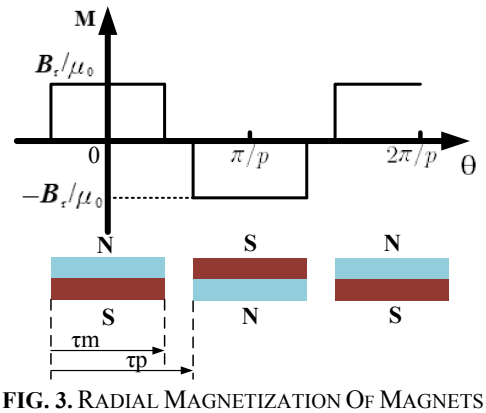

FIG. 3. RADIAL MAGNETIZATION OF MAGNETS

The field vectors B and H in all subdomains are by

$$\vec{B}(r,\theta) = B_r(r,\theta)\widehat{a_r} + B_\theta(r,\theta)\widehat{a_\theta} \quad (1)$$

$$\vec{H}(r,\theta) = H_r(r,\theta)\widehat{a_r} + H_\theta(r,\theta)\widehat{a_\theta} \quad (2)$$

Where, $\widehat{a_r}$ and $\widehat{a_\theta}$ are the normal vectors.

2.2. Governing Equations and Boundary Conditions
the whole domain of magnetic field can be divided into four subdomains, Permanent magnets (Region 1), air gap (Region 2), stator core (Region3) and Outer region (Region4), As shown in **FIG. 1**.
the governing equations of the scalar potential distributions for each subdomain in the r-θ coordinate system, are:

$$\frac{\partial^2 A_{z1}}{\partial r^2}+\frac{1}{r}\frac{\partial A_{z1}}{\partial r}+\frac{1}{r^2}\frac{\partial^2 A_{z1}}{\partial \theta^2}=\frac{1}{\mu_{rm}}\nabla.\vec{M} \quad (3)$$

$$\frac{\partial^2 A_{zi}}{\partial r^2}+\frac{1}{r}\frac{\partial A_{zi}}{\partial r}+\frac{1}{r^2}\frac{\partial^2 A_{zi}}{\partial \theta^2}=0 \text{ , for } i=2,3,4 \quad (4)$$

Where, In polar coordinates, the magnetization $\vec{M}$ is given by[15]

$$\vec{M}=M_r\widehat{a_r}+M_\theta\widehat{a_\theta} \quad (5)$$

For radial magnetization, can be expressed in coordinate as [1]:

$$M_r=\sum_n^\infty M_c(n)\cos n\theta+M_s(n)\ \sin n\theta \quad (6)$$

$$M_\theta=0 \quad (7)$$

Where

$$M_c(n)=M_n\cos n\omega t \quad (8)$$

$$M_s(n)=M_n\sin n\omega t \quad (9)$$

$$M_n=4p\frac{B_r}{n\pi\mu_0}\sin(n\pi\alpha_p/2p) \quad n/p=1,3,5,\ldots \quad (10)$$

p is the number of magnet pole pairs, and α_p is pole-arc to pole-pitch ratio.
The field vectors, the flux density and the field intensity, are written as TABLE 8. The radial component and tangential component of the field intensity described by the scalar potential are expressed as:

$$\vec{H}(r,\theta)=-\nabla\vec{A}(r,\theta)=-(\frac{\partial A}{\partial r}\widehat{a_r}+\frac{1}{r}\frac{\partial A}{\partial\theta}\widehat{a_\theta}) \quad (11)$$

$$H_r(r,\theta)=-\frac{\partial A}{\partial r} \quad (12)$$

$$H_\theta(r,\theta)=-\frac{1}{r}\frac{\partial A}{\partial\theta} \quad (13)$$

$$\overrightarrow{B_1}=\mu_0\mu_{rm}\overrightarrow{H_1}+\mu_0\vec{M} \quad (14)$$

$$B_{r1}(r,\theta)=\mu_0\mu_{rm}H_{r1}+\mu_0M_r=-\mu_0\mu_{rm}\frac{\partial A_1}{\partial r}+\mu_0M_r \quad (15)$$

$$B_{\theta1}(r,\theta)=\mu_0\mu_{rm}H_{\theta1}+\mu_0M_\theta=-\mu_0\mu_{rm}\frac{1}{r}\frac{\partial A_1}{\partial\theta} \quad (16)$$

$$\overrightarrow{B_i}=\mu_0\overrightarrow{H_i},\ i=2,4 \quad (17)$$

$$B_{ri}(r,\theta)=\mu_0H_{ri}=-\mu_0\frac{\partial A_i}{\partial r},\ i=2,4 \quad (18)$$

$$B_{\theta i}(r,\theta)=\mu_0H_{\theta i}=-\mu_0\frac{1}{r}\frac{\partial A_i}{\partial\theta},\ i=2,4 \quad (19)$$

$$\overrightarrow{B_3}=\mu_0\mu_{rc}\overrightarrow{H_3} \quad (20)$$

$$B_{r3}(r,\theta)=\mu_0\mu_{rc}H_{r3}=-\mu_0\mu_{rc}\frac{\partial A_3}{\partial r} \quad (21)$$

$$B_{\theta3}(r,\theta)=\mu_0\mu_{rc}H_{\theta3}=-\mu_0\mu_{rc}\frac{1}{r}\frac{\partial A_3}{\partial\theta} \quad (22)$$

The surface of the rotor yoke and the interface between the magnets and the air gap are, respectively, described by[15]

$$f_{rotor}(r,\theta)=r-R_r=0 \quad (23)$$

$$f_{magnet\text{-}gap}(r,\theta)=r-R_m=0 \quad (24)$$

The normalized vectors of these boundaries are respectively, described by

$$n_{rotor}(r,\theta)=\nabla f_{rotor}=\widehat{a_r} \quad (25)$$

$$n_{magnet\text{-}gap}(r,\theta)=\nabla f_{rotor}=\widehat{a_r} \quad (26)$$

The boundary condition along the surface of the rotor yoke, the interface between the magnets and the air gap, the interface between the air gap and stator, and the interface between the stator and outer region, are respectively, described by:

$$n_{rotor}\times H_1=0 \quad (27)$$

$$n_{magnet\text{-}gap}\times(H_1\text{-}H_2)=0 \quad (28)$$

$$n_{magnet\text{-}gap}.(B_1\text{-}B_2)=0 \quad (29)$$

$$n_{gap\text{-}stator}\times(H_2\text{-}H_3)=0 \quad (30)$$

$$n_{gap\text{-}stator}.(B_2\text{-}B_3)=0 \quad (31)$$

$$n_{stator\ yoke\text{-}air}\times(H_3\text{-}H_4)=0 \quad (32)$$

$$n_{stator\ yoke\text{-}air}.(B_3\text{-}B_4)=0 \quad (33)$$

$$n_{air}\times(H_4)=0 \quad (34)$$

$$n_{air}.(B_4)=0 \quad (35)$$

The general solutions of above equations are given by:

$$A_{z1}^{(0)}=\sum_n\left(A_1^{(0)}(n)r^n+B_1^{(0)}(n)r^{-n}+\frac{M_{Ac}(n)r}{\mu_{rm}}\right).\cos n\theta+\sum_n\left(C_1^{(0)}(n)r^n+D_1^{(0)}(n)r^{-n}+\frac{M_{As}(n)r}{\mu_{rm}}\right).\sin n\theta \quad (36)$$

$$A_{zi}^{(0)}=\sum_n\left(A_i^{(0)}(n)r^n+B_i^{(0)}(n)r^{-n}\right).\cos n\theta+\sum_n\left(C_i^{(0)}(n)r^n+D_i^{(0)}(n)r^{-n}\right).\sin n\theta \quad (37)$$

Also, $i=2,3,4$, n is the harmonic orders and coefficients of $A_1^{(0)}(n)$ – $A_4^{(0)}(n)$, $B_1^{(0)}(n)$ – $B_4^{(0)}(n)$, $C_1^{(0)}(n)$ – $C_4^{(0)}(n)$ and $D_1^{(0)}(n)$ – $D_4^{(0)}(n)$ are to be calculated by the boundary conditions.
The boundary condition to the surface of the rotor yoke, the interface between the magnets and the air gap, the interface between the air gap and stator, and the interface between the stator and outer region are obtained by the following expressions:

$$\frac{\partial A_{z1}^{(0)}}{\partial\theta}|_{r=R_r}=0 \quad (38)$$

$$\frac{\partial A_{z1}^{(0)}}{\partial\theta}|_{r=R_m}=\frac{\partial A_{z2}^{(0)}}{\partial\theta}|_{r=R_m} \quad (39)$$

$$-\mu_{rm}\frac{\partial A_{z1}^{(0)}}{\partial r}|_{r=R_m} + M_r = -\frac{\partial A_{z2}^{(0)}}{\partial r}|_{r=R_m} \quad (40)$$

$$\frac{\partial A_{z2}^{(0)}}{\partial \theta} = \frac{\partial A_{z3}^{(0)}}{\partial \theta}_{|r=R_{si}} \quad (41)$$

$$\frac{\partial A_{z2}^{(0)}}{\partial r} = \mu_{rc}\frac{\partial A_{z3}^{(0)}}{\partial r}_{|r=R_{si}} \quad (42)$$

$$\frac{\partial A_{z3}^{(0)}}{\partial \theta}_{|r=R_{so}} = \frac{\partial A_{z4}^{(0)}}{\partial \theta}_{|r=R_{so}} \quad (43)$$

$$\mu_{rc}\frac{\partial A_{z3}^{(0)}}{\partial r}_{|r=R_{so}} = \frac{\partial A_{z4}^{(0)}}{\partial r}_{|r=R_{so}} \quad (44)$$

$$\frac{\partial A_{z4}^{(0)}}{\partial \theta}_{|r=R_o} = 0 \quad (45)$$

$$\frac{\partial A_{z4}^{(0)}}{\partial r}_{|r=R_o} = 0 \quad (46)$$

Using the above boundary condition, the following expressions are obtained;

$$K_{11}^{(0)}A_1^{(0)} + K_{12}^{(0)}B_1^{(0)} = Y_1^{(0)} \quad (47)$$

$$K_{23}^{(0)}C_1^{(0)} + K_{24}^{(0)}D_1^{(0)} = Y_2^{(0)} \quad (48)$$

$$K_{31}^{(0)}A_1^{(0)} + K_{32}^{(0)}B_1^{(0)} + K_{35}^{(0)}A_2^{(0)} + K_{36}^{(0)}B_2^{(0)} = Y_3^{(0)} \quad (49)$$

$$K_{43}^{(0)}C_1^{(0)} + K_{44}^{(0)}D_1^{(0)} + K_{47}^{(0)}C_2^{(0)} + K_{48}^{(0)}D_2^{(0)} = Y_4^{(0)} \quad (50)$$

$$K_{51}^{(0)}A_1^{(0)} + K_{52}^{(0)}B_1^{(0)} + K_{55}^{(0)}A_2^{(0)} + K_{56}^{(0)}B_2^{(0)} = Y_5^{(0)} \quad (51)$$

$$K_{63}^{(0)}C_1^{(0)} + K_{64}^{(0)}D_1^{(0)} + K_{67}^{(0)}C_2^{(0)} + K_{68}^{(0)}D_2^{(0)} = Y_6^{(0)} \quad (52)$$

$$K_{75}^{(0)}A_2^{(0)} + K_{76}^{(0)}B_2^{(0)} + K_{79}^{(0)}A_3^{(0)} + K_{7,10}^{(0)}B_3^{(0)} = 0 \quad (53)$$

$$K_{87}^{(0)}C_2^{(0)} + K_{88}^{(0)}D_2^{(0)} + K_{8,11}^{(0)}C_3^{(0)} + K_{8,12}^{(0)}D_3^{(0)} = 0 \quad (54)$$

$$K_{95}^{(0)}A_2^{(0)} + K_{96}^{(0)}B_2^{(0)} + K_{99}^{(0)}A_3^{(0)} + K_{9,10}^{(0)}B_3^{(0)} = 0 \quad (55)$$

$$K_{10,7}^{(0)}C_2^{(0)} + K_{10,8}^{(0)}D_2^{(0)} + K_{10,11}^{(0)}C_3^{(0)} + K_{10,12}^{(0)}D_3^{(0)} = 0 \quad (56)$$

$$K_{11,9}^{(0)}A_3^{(0)} + K_{11,10}^{(0)}B_3^{(0)} + K_{11,13}^{(0)}A_4^{(0)} + K_{11,14}^{(0)}B_4^{(0)} = 0 \quad (57)$$

$$K_{12,11}^{(0)}C_3^{(0)} + K_{12,12}^{(0)}D_3^{(0)} + K_{12,15}^{(0)}C_4^{(0)} + K_{12,16}^{(0)}D_4^{(0)} = 0 \quad (58)$$

$$K_{13,9}^{(0)}A_3^{(0)} + K_{13,10}^{(0)}B_3^{(0)} + K_{13,13}^{(0)}A_4^{(0)} + K_{13,14}^{(0)}B_4^{(0)} = 0 \quad (59)$$

$$K_{14,11}^{(0)}C_3^{(0)} + K_{14,12}^{(0)}D_3^{(0)} + K_{14,15}^{(0)}C_4^{(0)} + K_{14,16}^{(0)}D_4^{(0)} = 0 \quad (60)$$

$$K_{15,13}^{(0)}A_4^{(0)} + K_{15,14}^{(0)}B_4^{(0)} = 0 \quad (61)$$

$$K_{15,15}^{(0)}C_4^{(0)} + K_{15,16}^{(0)}D_4^{(0)} = 0 \quad (62)$$

where the coefficients of $A_i^{(0)}(n)$, $B_i^{(0)}(n)$, $C_i^{(0)}(n)$ and $D_i^{(0)}(n)$ in ith region are Column vectors and constructed in the same way, e.g. $A_i^{(0)} = \left[A_i^{(0)}(1), A_i^{(0)}(2), \cdots, A_i^{(0)}(N)\right]^T$, $N = n_{max}$ is the maximum spatial harmonic order considered in the flux density ,and

$$K_{11}^{(0)} = K_{23}^{(0)} = \mathrm{diag}(R_r, {R_r}^2, \cdots, {R_r}^N)$$

$$K_{12}^{(0)} = K_{24}^{(0)} = \mathrm{diag}({R_r}^{-1}, {R_r}^{-2}, \cdots, {R_r}^{-N})$$

$$K_{31}^{(0)} = -K_{35}^{(0)} = K_{43}^{(0)} = -K_{47}^{(0)} = \mathrm{diag}(R_m, {R_m}^2, \cdots, {R_m}^N)$$

$$K_{32}^{(0)} = -K_{36}^{(0)} = K_{44}^{(0)} = -K_{48}^{(0)} = \mathrm{diag}({R_m}^{-1}, {R_m}^{-2}, \cdots, {R_m}^{-N})$$

$$K_{51}^{(0)} = K_{63}^{(0)} = \mathrm{diag}(\mu_{rm}, 2\mu_{rm}R_m, \cdots, \mu_{rm}N{R_m}^{N-1})$$

$$K_{52}^{(0)} = K_{64}^{(0)} = \mathrm{diag}(-\mu_{rm}{R_m}^{-2}, -2\mu_{rm}{R_m}^{-3}, \cdots, -\mu_{rm}N{R_m}^{-N-1})$$

$$K_{55}^{(0)} = K_{67}^{(0)} = \mathrm{diag}(-1, -2R_m, \cdots, -N{R_m}^{N-1})$$

$$K_{56}^{(0)} = K_{68}^{(0)} = \mathrm{diag}({R_m}^{-2}, 2{R_m}^{-3}, \cdots, N{R_m}^{-N-1})$$

$$K_{75}^{(0)} = -K_{79}^{(0)} = K_{87}^{(0)} = -K_{8,11}^{(0)} = \mathrm{diag}(R_{si}, {R_{si}}^2, \cdots, {R_{si}}^N)$$

$$K_{76}^{(0)} = -K_{7,10}^{(0)} = K_{88}^{(0)} = -K_{8,12}^{(0)} = \mathrm{diag}({R_{si}}^{-1}, {R_{si}}^{-2}, \cdots, {R_{si}}^{-N})$$

$$K_{95}^{(0)} = -\frac{1}{\mu_{rc}}K_{99}^{(0)} = K_{10,7}^{(0)} = -\frac{1}{\mu_{rc}}K_{10,11}^{(0)} = \mathrm{diag}(1, R_{si}, \cdots, {R_{si}}^{N-1})$$

$$K_{96}^{(0)} = -\frac{1}{\mu_{rc}}K_{9,10}^{(0)} = K_{10,8}^{(0)} = -\frac{1}{\mu_{rc}}K_{10,12}^{(0)} = \mathrm{diag}(-{R_{si}}^{-2}, -{R_{si}}^{-3}, \cdots, -{R_{si}}^{-N-1})$$

$$K_{11,9}^{(0)} = -K_{11,13}^{(0)} = K_{12,11}^{(0)} = -K_{12,15}^{(0)} = \mathrm{diag}(R_{so}, {R_{so}}^2, \cdots, {R_{so}}^N)$$

$$K_{11,10}^{(0)} = -K_{11,14}^{(0)} = K_{12,12}^{(0)} = -K_{12,16}^{(0)} = \mathrm{diag}({R_{so}}^{-1}, {R_{so}}^{-2}, \cdots, {R_{so}}^{-N})$$

$$K_{13,9}^{(0)} = -\mu_{rc}K_{13,13}^{(0)} = K_{14,11}^{(0)} = -\mu_{rc}K_{14,15}^{(0)} = \mu_{rc}\mathrm{diag}(1, R_{so}, \cdots, {R_{so}}^{N-1})$$

$$K_{13,10}^{(0)} = -\mu_{rc}K_{13,14}^{(0)} = K_{14,12}^{(0)} = -\mu_{rc}K_{14,16}^{(0)} = \mu_{rc}\mathrm{diag}(-{R_{so}}^{-2}, -{R_{so}}^{-3}, \cdots, -{R_{so}}^{-N-1})$$

$$K_{15,13}^{(0)} = K_{15,15}^{(0)} = \mathrm{diag}(R_o, {R_o}^2, \cdots, {R_o}^N)$$

$$K_{15,14}^{(0)} = K_{15,16}^{(0)} = \mathrm{diag}({R_o}^{-1}, {R_o}^{-2}, \cdots, {R_o}^{-N})$$

$$K_{16,13}^{(0)} = K_{16,15}^{(0)} = \mathrm{diag}(1, R_o, \cdots, {R_o}^{N-1})$$

$$K_{16,14}^{(0)} = K_{16,16}^{(0)} = -\mathrm{diag}({R_o}^{-2}, {R_o}^{-3}, \cdots, {R_o}^{-N-1})$$

$$Y_1^{(0)} = -R_r/\mu_{rm}\left[M_{Ac}(1), M_{Ac}(2), \cdots, M_{Ac}(N)\right]^T$$

$$Y_2^{(0)} = -R_r/\mu_{rm}\left[M_{As}(1), M_{As}(2), \cdots, M_{As}(N)\right]^T$$

$$Y_3^{(0)} = -R_m/\mu_{rm}\left[M_{Ac}(1), M_{Ac}(2), \cdots, M_{Ac}(N)\right]^T$$

$$Y_4^{(0)} = -R_m/\mu_{rm}\left[M_{As}(1), M_{As}(2), \cdots, M_{As}(N)\right]^T$$

$$Y_5^{(0)} = \left[-M_{Ac}(1) + M_c(1), -M_{Ac}(2) + M_c(2), \cdots, -M_{Ac}(N) + M_c(N)\right]^T$$

$$Y_6^{(0)} = \left[-M_{As}(1) + M_s(1), -M_{As}(2) + M_s(2), \cdots, -M_{As}(N) + M_s(N)\right]^T$$

$$M_{Ac}(n) = \begin{cases} \frac{M_c(n)\ln r}{2} & n = 1 \\ \frac{M_c(n)}{1-n^2} & n = 2,3,\cdots \end{cases}$$

$$M_{As}(n) = \begin{cases} \frac{M_s(n)\ln r}{2} & n = 1 \\ \frac{M_s(n)}{1-n^2} & n = 2,3,\cdots \end{cases}$$

$$M_c(n) = M_n\cos n\omega t$$

$$M_s(n) = M_n\sin n\omega t$$

After solving the system of equations (47)-(62), Calculated the coefficients of $A_i^{(0)}(n)$, $B_i^{(0)}(n)$, $C_i^{(0)}(n)$,and $D_i^{(0)}(n)$ in ith region and based on (36), (37) We obtain the magnetic potential vector in all subdomains. Then, with the help of relations (11)-(22), the density vector and the intensity of the magnetic field can be determined in all sub-domains.

3. RESULTS AND DISCUSSION

The major parameters of the slot less PM machine in TABLE. 9 are used to the magnetic field.

TABLE. 9. THE MAJOR PARAMETERS

parameter	Value (unit)
R_r	100mm
R_m	110mm
Airgap distance	5mm
Stator thickness	70mm
Outer region thickness	70mm
μ_{rm}	1.05
μ_{rc}	2000
Magnet remanence	1.2 T
Magnetization type	radial
Rated speed	400rpm
α_p	1
p	4
Number of magnets	8

the flux density magnitude of the finite element simulation at all sub domains given in **FIG. 4**. The results show that, the distribution of the field in all points is symmetrical.

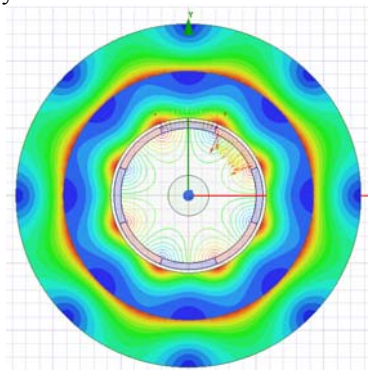

FIG. 4. THE FLUX DENSITY MAGNITUDE OF THE FINITE ELEMENT SIMULATION AT ALL SUBDOMAINS

The flux density distribution of the analytical model in the all subdomains compared with the FE predictions for the case of no rotor eccentricity are given in **FIG. 5 -FIG. 8**. As it is apparent in this figure, the prediction of the flux density in all subdomains are well matched in both the analytical model and the FE model, except for some peak values which determined by the harmonic order N.

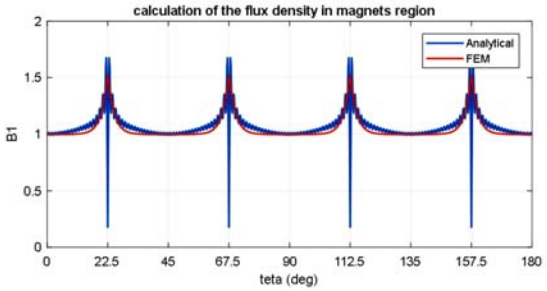

FIG. 5. THE FLUX DENSITY MAGNITUDE OF THE ANALYTICAL MODEL AND FE IN THE PMS REGION AT $R_1 = (R_R + R_M)/2$.

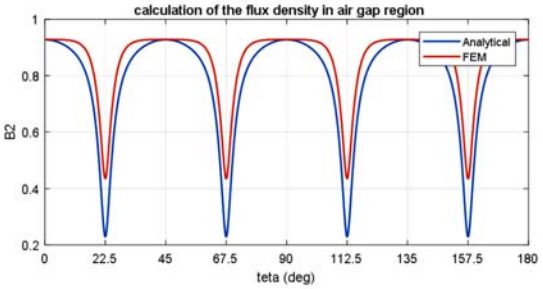

FIG. 6. THE FLUX DENSITY MAGNITUDE OF THE ANALYTICAL MODEL AND FE IN THE AIRGAP REGION AT $R_2 = (R_{SI} + R_M)/2$

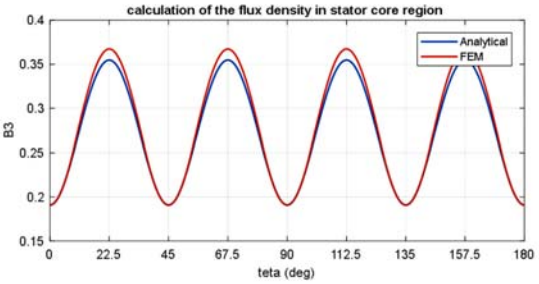

FIG. 7. THE FLUX DENSITY MAGNITUDE OF THE ANALYTICAL MODEL AND FE IN THE STATOR REGION AT $R_3 = (R_{SO} + R_{SI})/2$

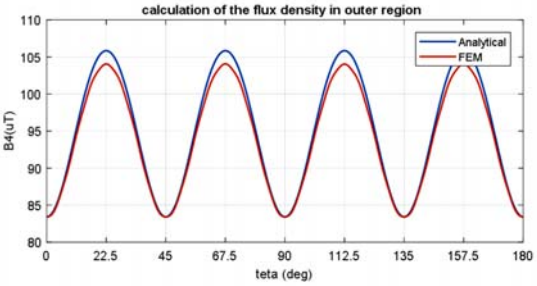

FIG. 8. THE FLUX DENSITY MAGNITUDE OF THE ANALYTICAL MODEL AND FE IN THE MOTOR OUTER REGION AT $R_4 = R_{SO} + 1^{cm}$

4. CONCLUSION

A general two-dimensional analytical subdomain model for predicting the field distribution of a SMPMSMs has been established and validated by finite element calculations in this paper. proposed model in search for considers, the effect of the rotor eccentricity with the help of the perturbation method, for calculate of field distribution in the all subdomains, in the next study. the magnetic field domain is divided into three subdomains, viz. magnets, air gap, stator core (slot less), and outer region. The model can be Modified to consider effect of slotting on the field distribution. Although the method has been applied to SMPMSMs it is equally applicable to brushless permanent magnet ac motors. It is clear that the results of the analytical prediction are in close accordance with those realized by tow-dimensional FEM. The results indicate that, the analytical model well matches the finite-element prediction, except for some peak values which determined by the harmonic order N. In two respects, this finding makes an important contribution to the improvement of earlier work. First, it corroborates the findings of previous how found that the subdomain model can accurately predict the open-circuit magnetic field in surface-mounted permanent-magnet machines. Second, it demonstrates that, the magnetic field leaks out symmetrically and by measuring it, the eccentricity fault can be detected. Though this study provides evidence that Calculation of leak fields plays a significant role in Detection of Eccentricity Fault in PM machines, the reader should note its limitations and the ways in which future research might be enhanced. variables that was not investigated her was the effect of stator slots, stator windings and Electromagnetic noise of the environment. There is clearly much room for further research in this respect.

5. REFERENCES

[1]. Zhu, Z.Q., L.J. Wu, and Z.P. Xia, An Accurate Subdomain Model for Magnetic Field Computation in Slotted Surface-Mounted Permanent-Magnet Machines. *IEEE Transactions on Magnetics*, 2010. 46(4): p. 1100-1115.

[2]. Frédéric Dubas, K.B., New Scientific Contribution on the 2-D Subdomain Technique in Polar Coordinates: Taking into Account of Iron Parts. *Math*. *Comput*. *Appl*, 2017. 22.

[3]. Chau, K., Electric vehicle machines and drives: design, analysis and application. 2015: *John Wiley & Sons.*

[4]. Gieras, J.F., R.-J. Wang, and M.J. Kamper, Axial flux permanent magnet brushless machines. 2008: *Springer Science & Business Media*.

[5]. Sprangers, R., et al., Magnetic saturation in semi-analytical harmonic modeling for electric machine analysis. *IEEE Transactions on Magnetics*, 2015. 52(2): p. 1-10.

[6]. Theodoulidis, T. and J. Bowler, Eddy-current interaction of a long coil with a slot in a conductive plate. *IEEE Transactions on Magnetics*, 2005. 41(4): p. 1238-1247.

[7]. Jabbari, A. and F. Dubas, A New Subdomain Method for Performances Computation in Interior Permanent-Magnet (IPM) Machines. *Iranian Journal of Electrical and Electronic Engineering,* 2020. 16(1): p. 26.

[8]. Rezaee-Alam, F., B. Rezaeealam, and J. Faiz, Unbalanced Magnetic Force Analysis in Eccentric Surface Permanent-Magnet Motors Using an Improved Conformal Mapping Method. *IEEE Transactions on Energy Conversion*, 2017. 32(1): p. 146-154.

[9]. Li, Y.X. and Z.Q. Zhu, Cogging Torque and Unbalanced Magnetic Force Prediction in PM Machines With Axial-Varying Eccentricity by Superposition Method. *IEEE Transactions on Magnetics*, 2017. 53(11): p. 1-4.

[10]. Li, Y., Q. Lu, and Z.-Q. Zhu, Unbalanced magnetic force prediction in permanent magnet machines with rotor eccentricity by improved superposition method. *IET Electric Power Applications*, 2017. 11(6): p. 1095-1104.

[11]. Hu, H., et al., No-Load Magnetic Field and Cogging Force Calculation in Linear Permanent-Magnet Synchronous Machines With Semiclosed Slots. *IEEE Transactions on Industrial Electronics*, 2017. 64(7): p. 5564-5575.

[12]. Faiz, J. and E. Mazaheri-Tehrani, Demagnetization Modeling and Fault Diagnosing Techniques in Permanent Magnet Machines Under Stationary and Nonstationary Conditions: An Overview. *IEEE Transactions on Industry Applications*, 2017. 53(3): p. 2772-2785.

[13]. Lin, F. and S. Zuo. Influence of rotor eccentricity on electromagnetic vibration and noise in permanent-magnet synchronous motor with different slot-pole combinations. in *Proceedings of Meetings on Acoustics* 172ASA. 2016. ASA.

[14]. Le Besnerais, J., Q. Souron, and E. Devillers, Analysis of the electromagnetic acoustic noise and vibrations of a high-speed brushless DC motor. 2016.

[15]. Fu, J. and C. Zhu, Subdomain Model for Predicting Magnetic Field in Slotted Surface

Mounted Permanent-Magnet Machines With Rotor Eccentricity. *IEEE Transactions on Magnetics*, 2012. 48(5): p. 1906-1917.

[16]. Wu, L., et al., Analytical prediction of electromagnetic performance of surface-mounted PM machines based on subdomain model accounting for tooth-tips. *IET Electric Power Applications*, 2011. 5(7): p. 597-609.

[17]. Zhu, Z., L. Wu, and Z. Xia, An accurate subdomain model for magnetic field computation in slotted surface-mounted permanent-magnet machines. *IEEE Transactions on Magnetics*, 2009. 46(4): p. 1100-1115.

[18]. Faiz, J., A new hybrid analytical model based on winding function theory for analysis of surface mounted permanent magnet motors. COMPEL - *The international journal for computation and mathematics in electrical and electronic engineering,* 2019. 38(2): p. 745-758.

[19]. Zhang, Z., et al. An Equivalent Magnetic Circuit Model of PMSM Demagnetization Fault. *in IOP Conference Series: Materials Science and Engineering*. 2019. IOP Publishing.

[20]. Dubas, F. and K. Boughrara, New scientific contribution on the 2-D subdomain technique in Cartesian coordinates: taking into account of iron parts. *Mathematical and Computational Applications*, 2017. 22(1): p. 17.

[21]. Rahideh, A. and T. Korakianitis, Analytical Open-Circuit Magnetic Field Distribution of Slotless Brushless Permanent-Magnet Machines With Rotor Eccentricity. *IEEE Transactions on Magnetics*, 2011. 47(12): p. 4791-4808.

[22]. Kumar, P. and P. Bauer, Improved Analytical Model of a Permanent-Magnet Brushless DC Motor. *IEEE Transactions on Magnetics,* 2008. 44(10): p. 2299-2309.

[23]. Han, T., et al., Bearing fault identification based on convolutional neural network by different input modes. *Journal of the Brazilian Society of Mechanical Sciences and Engineering,* 2020. 42(9): p. 474.

[24]. Azeem, B., et al., Synchronous and a-synchronous machines (SAASMs): rotor and stator faults. *Engineering and Applied Science Letter*, 2019. 2(2): p. 01 – 09.

[25]. Xu, X., Q. Han, and F. Chu, Review of electromagnetic vibration in electrical machines. *Energies*, 2018. 11(7): p. 1779.

[26]. Usman, A., B.M. Joshi, and B.S. Rajpurohit. Review of fault modeling methods for permanent magnet synchronous motors and their comparison. *in 2017 IEEE 11th International Symposium on Diagnostics for Electrical Machines, Power Electronics and Drives (SDEMPED)*. 2017.

[27]. Fekry, M., et al., A Comprehensive performance assessment of the integration of magnetic bearings with horizontal axis wind turbine. *Mathematics and Computers in Simulation,* 2019. 156: p. 1-39.

[28]. Çıra, F., Detection of eccentricity fault based on vibration in the PMSM. *Results in Physics,* 2018. 10: p. 760-765.

[29]. Lin, F., S. Zuo, and W. Deng, Impact of rotor eccentricity on electromagnetic vibration and noise of permanent magnet synchronous motor. *Journal of Vibroengineering,* 2018. 20(2).

[30]. Zhang, A., et al., Analysis of Nonlinear Vibration in Permanent Magnet Synchronous Motors under Unbalanced Magnetic Pull. *Applied Sciences*, 2018. 8(1): p. 113.

[31]. Lin, F., et al., Reduction of vibration and acoustic noise in permanent magnet synchronous motor by optimizing magnetic forces. *Journal of Sound and Vibration*, 2018. 429: p. 193-205.

[32]. He, H., et al., Tolerance analysis of electrified vehicles on the motor demagnetization fault: From an energy perspective. *Applied Energy*, 2018. 227: p. 239-248.

[33]. McCloskey, A., et al., Analytical calculation of vibrations of electromagnetic origin in electrical machines. *Mechanical Systems and Signal Processing*, 2018. 98: p. 557-569.

[34]. Hekmati, A., Aliahmadi. M, Double-layer rotor magnetic shield performance analysis in high temperature superconducting synchronous generators under short circuit fault conditions, *Cryogenics*, 2016. 80: p. 147-153.

[35]. Kim, S.J., et al., Transfer Torque Performance Comparison in Coaxial Magnetic Gears With Different Flux-Modulator Shapes. *IEEE Transactions on Magnetics*, 2017. 53(6): p. 1-4.

[36]. Singh, A., et al., A review of induction motor fault modeling. *Electric Power Systems Research*, 2016. 133: p. 191-197.

[37]. Kim, D., M.D. Noh, and Y. Park, Unbalanced Magnetic Forces Due to Rotor Eccentricity in a Toroidally Wound BLDC Motor. *IEEE Transactions on Magnetics*, 2016. 52(7): p. 1-4.

[38]. Hekmati. A., A novel acoustic method of partial discharge allocation considering structure-borne waves. *International Journal*

of Electrical Power & Energy Systems, 2016. 77: p. 250-255.

[39]. Kim, U. and D.K. Lieu, Magnetic field calculation in permanent magnet motors with rotor eccentricity: with slotting effect considered. *IEEE Transactions on Magnetics,* 1998. 34(4): p. 2253-2266.